NIPPON STEEL TECHNICAL REPORT No. 122 NOVEMBER 2019

UDC 629 . 11 . 011 : 678 . 664

Technical Report

Technologies and Application Examples for Weight Reduction of Vehicle Frames

Satoshi HIROSE*

Abstract

In order to achieve both collision safety and further weight reduction of vehicle frames, it is necessary to undertake design in combination with fundamental technology considering high strength and influence of thinning of steel sheet in terms of performance. In this report, two examinations of lightweight body frames are introduced. The first is to reduce the weight when a foamed resin material is used in combination with a front side member for the purpose of controlling out-of-plane deformation due to compressive load. The second is to reduce the weight when the optimum arrangement of the material strength and the steel sheet thickness is applied to an outer center pillar.

1. Introduction

To achieve both collision safety and further weight reduction of vehicle bodies for reducing environmental stress in future, ultra-high-strength steel with a tensile strength exceeding 980 MPa has been used as a material for many body frames. To further reduce the weight of vehicle bodies, it is effective to reduce the thickness of steel sheets to be applied to body frames while satisfying the required performance. However, thinner sheets tend to cause out-of-plane deformation on body frames, which may reduce the rigidity and may change the deformation mode when vehicles come into collision. Therefore, in addition to simple replacement of materials, it is desirable to develop vehicle bodies by, for example, improving the cross-sectional shapes of frames and arranging necessary materials at appropriate places in order to draw the best out of the materials applied. Such technologies are required to further reduce the weight of vehicle bodies.

This paper focuses on phenomena in collision of vehicle bodies and describes lightweight body frames with excellent crash performance. Next, Chapter 2 describes lightweight front side members and Chapter 3 describes lightweight center pillars.

2. Development of Lightweight Front Side Members for which Resin Materials are used in Combination

2.1 Discussed models

Front side members (FSMs) are key body frames to secure collision safety at the time of frontal collision (e.g., full-wrap collision[1] and offset collision[2]). Therefore, the deformation behavior of such members should desirably be stable, that is to say, they should absorb the striking energy from collision stably. To suppress out-of-plane deformation that is a cause of changes in deformation behavior, FSMs containing foamed resins were studied.

Figure 1a illustrates a base FSM in the shape of the letter “S.” When the FSM receives a load in the axial direction of the frame and deforms, it bends sharply (hereinafter simply referred to as “bend”) at the two curves of the letter “S” (hereinafter referred to as “two-section bending”) as its deformation behavior (**Fig. 2**). **Table 1** shows the applicable steel sheet (base model in Table 1) when the stable deformation shown in Fig. 2 occurs.

2.2 Influence of weight reduction by simple replacement of materials

To reduce the weight of FSMs mentioned in the previous section, Nippon Steel Corporation tried to reduce the weight by thinning 2 to 3 gauges (approximately 0.4 to 0.6 mm). Weight reduction of 2 to 3 gauges corresponds to weight reduction of approximately 30% (model A in Table 1). To secure resistance to impact, a steel sheet whose tensile strength is higher by approximately 400 MPa was used and the axial strength and fully plastic bending moment of the cross section of the body frame were set to be equivalent to those of the base model.

Compressive force was given in the axial directions of the base model, model A, and model C (shown in **Fig. 1b**) (Table 1) to evaluate the crash performance. Specifically, the end of each model was brought into contact with a special tool in a U-shape that covered

* Senior Researcher, Ph.D., Kimitsu R & D Lab.
1 Kimitsu, Kimitsu City, Chiba Pref. 299-1141

the end (Fig. 2). Forced deformation was given in the axial direction at a constant speed (6 m/s) and the volume of forced deformation (stroke) and load (force) were evaluated by computer-aided engineering (CAE). Model C was prepared by adding a trim hole for guiding bending and reinforcement (R/F) to model A. The R/F was very thin and its strength was low, so it hardly contributed to the axial strength and fully plastic bending moment (Table 1). In this paper, the energy absorption amount (hereinafter referred to as "EA") when the stroke is 200 mm (when the deformation is approximately 67% of the length of the body frame) is used as an index for crash performance.

Figure 3 shows the loading history and **Fig. 4** shows the EA history. For the base model and models A and C, the force peaks are seen immediately before bending and the force rapidly decreases after bending. This rapid decrease in force may be caused because the cross sections of the body frames suddenly crash due to abrupt deformation concentration at the bent sections, which significantly reduces the second moment of area, in other words, which reduces the flexural rigidity. The figure shows that the same phenomenon occurs in all models. However, the degrees of the deformation resistance vary. The deformation resistance of models A and C is smaller than that of the base model immediately before bending deformation, in particular. As a result, the difference in the EA between the base model and the other two models becomes larger around the initial force peak (within a stroke of 50 mm). When the stroke is 200 mm, the difference is approximately 2.4 kJ for model A and approximate-

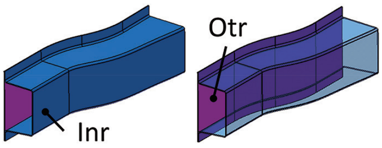

Fig. 1a Base model and model A

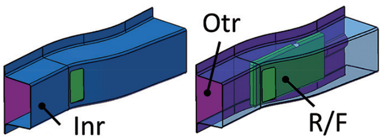

Fig. 1b Model C

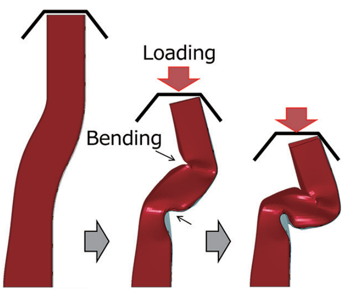

Fig. 2 Deformation behavior of S-shaped frame

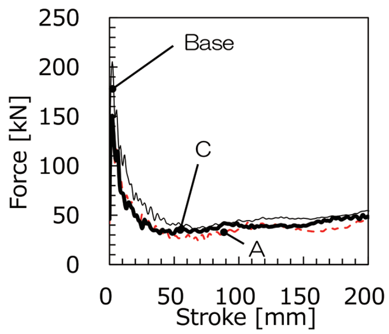

Fig. 3 History of loading and deformation

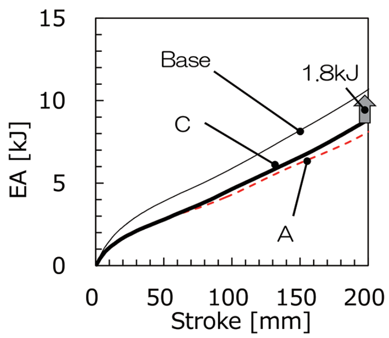

Fig. 4 History of absorbed energy and deformation

Table 1 Applicable materials and performance of each model

Model	Base	A	B1	B2	B3	C
Inr Tensile strength/thickness	780 MPa /2.0 mm	1180 MPa /1.4 mm	1180 MPa /1.4 mm	1180 MPa /1.4 mm	1180 MPa /1.4 mm	1180 MPa /1.4 mm
Otr Tensile strength/thickness	690 MPa /1.5 mm	1180 MPa /1.0 mm	1180 MPa /1.0 mm	1180 MPa /1.0 mm	1180 MPa /1.0 mm	1180 MPa /1.0 mm
R/F Tensile strength/thickness	–	–	–	–	270 MPa /0.5 mm	270 MPa /0.5 mm
Resin material	–	–	Urethane foam *3 times type	Urethane foam *3 times type	Urethane foam *3 times type	–
Axial strength	507 kN	507 kN (+0%)	522 kN (+3%)	522 kN (+3%)	520 kN (+3%)	517 kN (+2%)
Fully plastic bending moment	15.1 kNm	15.1 kNm (+0%)	15.4 kNm (+2%)	15.4 kNm (+2%)	15.8 kNm (+4%)	15.7 kNm (+4%)
Weight	3.4 kg	2.3 kg (−32%)	3.7 kg (+11%)	3.0 kg (−10%)	2.6 kg (−25%)	2.4 kg (−29%)

ly 1.8 kJ for model C.

Model C has a steel R/F, but it did not contribute to obvious performance improvement and the performance was at the same level. This result shows that deformation behavior in the early stage of deformation where elastic deformation is dominant causes larger differences in the crash performance than deformation behavior after bending deformation involving large deformation where plastic deformation is dominant. One possible cause is differences in out-of-plane deformation. Regarding in-plane deformation, the influence of thickness reduction can be eliminated through enhancement of strength. On the other hand, out-of-plane deformation where bending deformation is dominant may be encouraged by thickness reduction of the steel sheets, which may result in lower flexural rigidity of the body frame.

2.3 Study of lightweight body frames

As measures to improve the crash performance of models A and C without changing the steel type applied, the author considered that key points were (i) suppression of out-of-plane deformation, (ii) suppression of abrupt crash of the cross section in large deformation, and (iii) maintaining of deformation behavior (two-section bending in this paper) and studied lightweight body frames.

First, to suppress out-of-plane deformation, the out-of-plane force when axial compressive force was applied to a body frame was calculated. Specifically, a case where axial compression is applied to a square sheet as shown in **Fig. 5** was studied. This assumes an area between the ridgelines of a body frame. Both sides of this sheet were constrained in the width direction (direction Y in the figure) and in the out-of-plane direction (direction Z in the figure). A load (Fx) was applied from above in the axial direction (direction X in the figure). The lower end was constrained only in the axial direction. For simplification, for the width direction, minute initial deflection in the out-of-plane direction is expressed by formula (1).

$$\omega(y) = \omega_0 \sin\left(\frac{\pi y}{L}\right). \tag{1}$$

Here, ω_0 is the initial deflection at the center in the width direction and L is the length in the width direction. The largest out-of-plane deformation occurs at the center in the width direction in the deformation mode in formula (1). Fz is defined as out-of-plane force that works to prevent such out-of-plane deformation caused by the axial compressive force (Fx). Formula (2) shows the relationship between Fx and Fz.

$$\frac{1}{Fz} = \frac{L^2}{48EI\omega_0}\left\{\frac{cf_y^E}{\mu}\left(\frac{1}{F\mathrm{x}}\right) - 1\right\}. \tag{2}$$

Here, E is Young's modulus, μ is Poisson's ratio, and I is the second moment of area. In addition, c is the effective width for the axial-direction load (Fx), and f_y^E is the buckling load for the width-direction load in the unit of length. They are shown as formulas (3) and (4).[3)]

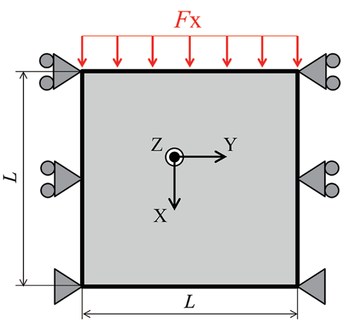

Fig. 5 Out-of-plane load evaluation model

Formula (2) finally transforms into formula (5).

$$f_y^E = \frac{\pi^2 EI}{L^2}, \tag{3}$$

$$c = 2t\sqrt{\frac{\pi^2 E}{12(1-\mu^2)\sigma_0}}, \tag{4}$$

$$\frac{1}{Fz} = \frac{1}{48\omega_0}\left\{\left(\frac{2\pi^3 t}{\mu}\sqrt{\frac{E}{12(1-\mu^2)\sigma_0}}\right)\left(\frac{1}{F\mathrm{x}}\right) - 1\right\}. \tag{5}$$

Here, t is the thickness and σ_0 is the yield stress. Formula (5) shows that the relationship between the axial compressive force (Fx) and out-of-plane force (Fz) does not rely on the size of the sheet. When the ratio of Fz to Fx (Fz/Fx) is calculated, the relationship can be summarized as shown in **Table 2**. Condition 1 assumes a general body frame made from ultra-high-strength steel. The table shows that the out-of-plane force (Fz) is very small at approximately 1/240 of the axial compressive force (Fx). In addition, formula (5) shows that the out-of-plane force (Fz) tends to increase when the thickness decreases, that the strength is enhanced, and that the initial deflection increases. However, for example, even when the thickness is halved as estimated largely, the out-of-plane force (Fz) is still small at approximately 1/60 of the axial compressive force (Fx) (condition 2 in Table 2).

Moreover, the table shows when the initial shape of a sheet is poor and when it has large initial deflection with a size of approximately half of the thickness at the center in the width direction, the ratio is small at approximately 1/50 (condition 4 in Table 2). That is to say, large force may not be required to suppress out-of-plane deformation. For example, when a body frame having a rectangular cross section made from the material under condition 1 in Table 2 receives up to 200 kN of axial compressive force, approximately 50 kN of axial compressive force is applied to each plane. Therefore, it is sufficient to apply approximately 0.2 kN at maximum to suppress out-of-plane deformation in the range corresponding to the length in the width direction.

Therefore, for example, when a urethane resin material whose Young's modulus is much smaller than that of the iron is used, it is difficult to support large axial force, but out-of-plane deformation may be sufficiently suppressed as described above. Given this situation, to suppress out-of-plane deformation, urethane resin was arranged in three patterns using model C mentioned above (**Fig. 6**). The urethane resin to be used was foamed at ordinary temperature and contained in model C. Model B1 has no R/F, whereas model C has, and the inside is filled with resin. Model B2 has no R/F unlike model C and resin is provided only at the curvature section at which bending deformation occurs in consideration of (ii) above. For model B3 prepared based on model C, no resin material is provided at the locations at which bending may occur at the curvature section so as not to hinder bending deformation in consideration of (ii) and

Table 2 Relationship between axial force and out-of-plane force

Condition	1	2	3	4
Yield stress	600 MPa	600 MPa	1200 MPa	600 MPa
Thickness	1.0 mm	0.5 mm	1.0 mm	1.0 mm
Elastic modulus	206 GPa	206 GPa	206 GPa	206 GPa
Poisson's ratio	0.3	0.3	0.3	0.3
Initial deflection	0.1 mm	0.1 mm	0.1 mm	0.5 mm
Fz/Fx	1/240	1/60	1/170	1/50

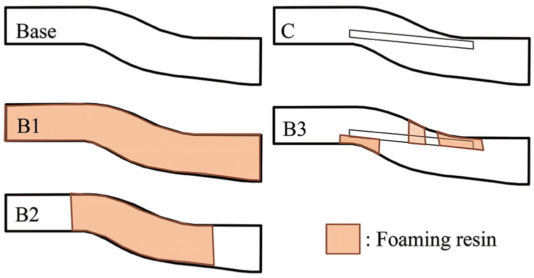

Fig. 6 Front side member models studied

(iii), but resin has been arranged around the section.

As deformation behavior, bending deformation advances involving deformation around the bent section, so even when resin material is provided around the bent sections instead of the bent sections themselves, it can be expected that the cross-sectional collapse deformation in (ii) above is sufficiently suppressed. In addition, resin material is provided only inside the bent section in bending deformation, so the R/F is effectively used as a threshold. Model B1 is rather heavier than the base model, so it can be understood that resin needs to be arranged in an appropriate way (Table 1). The thickness of the resin material filling was adjusted such that the flexural rigidity of the plane with which the resin material was in contact was the same level as that of the base model.

2.4 Verification of lightweight body frames

The crash performance of the models described in the previous section was evaluated by testing. Among the models described in the previous section, the base model and models B1, B2, B3, and C were actually prepared. A 590-MPa, 1.6-mm-thick steel sheet was used for the Otr of the base model prepared in this study (Fig. 1a). A 980-MPa, 1.0-mm-thick steel sheet was used for the Otr of models B1, B2, B3, and C (Fig. 1b). The axial strength and fully plastic bending moment were almost the same for all the models. As shown in Fig. 2 in 2.2, compressive force was applied in the axial direction for evaluation. Specifically, improvement of performance thanks to the resin material was evaluated. In other words, improvement of EA was evaluated. The targeted improvements (increase in the EA) were 2.4 kJ for models B1 and B2 without an R/F prepared based on model C as described in 2.2 and 2.3, and 1.8 kJ for model B3 with an R/F prepared based on model C. The test speed was constant (1 mm/s) and forced displacement was given. The volume of forced displacement (stroke) and reaction force were measured. **Figure 7** are photographs taken in the actual test. The urethane resin material used in this test was the 3 times type (Penguin Foam #3360 (3 times type) made by Sunstar Engineering Inc.) in **Table 3**.

The bending point of models C, B1, and B3 may be almost the same as that of the base model. However, the figure shows that B2 bent near the upper and lower ends, not at the curvature section unlike models C, B1, and B3. In addition, the spot-welded section on model B1 broke in the course of deformation and that served as the starting point of a crack on the material, allowing the inside resin material to escape. This may be because the inside of model B1 was fully packed with resin, which suppressed the cross-sectional deformation caused by bending deformation excessively, resulting in increase in load to the spot-welded section.

Next, **Fig. 8** shows the relationship between the EA and weight reduction rate when the stroke is 200 mm. The performance of model B1 was significantly improved thanks to the resin material, but the weight also increased. For model B2, the weight reduction rate is expected to be approximately 10%, but the deformation behavior significantly changed, not achieving the target. Meanwhile, model B3 satisfied the target and the weight reduction rate is large at approximately 25%, indicating that lightweight body frames with high crash performance can be made in combination with resin materials. In addition, comparison was performed between the values obtained by dividing the increased EA by the increased weight (EA improvement efficiency) for the models (**Fig. 9**). Compared with the result of the case where only the thicker steel sheet was used, the EA improvement efficiency of the cases using the resin material is higher. The graph also shows that arranging the resin material at appropriate places can enhance the EA improvement efficiency.

Thirdly, to see the influence of resin characteristics on model B3, other types of resin material were tested in a similar way. The used foamed resin materials were Penguin Foam #3360 (3 times type, 5 times type, and 10 times type) and Penguin Foam #3340 (vibrational

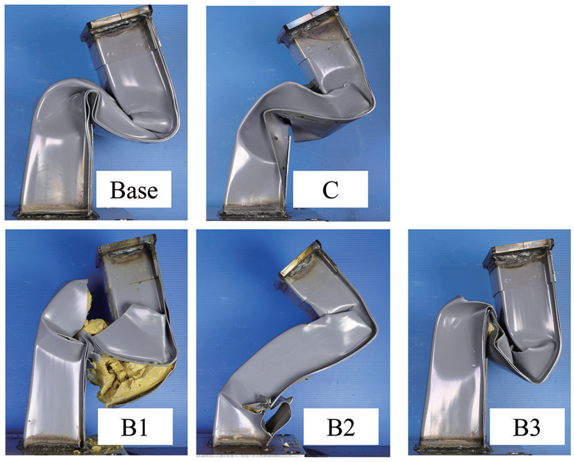

Fig. 7 Pictures of each model after the test

Table 3 Material properties of foamed resin

Foaming resin	Density	Compressive elastic modulus
3 times type	350 kg/m³	220 MPa
5 times type	250 kg/m³	120 MPa
10 times type	110 kg/m³	40 MPa
Vibrational absorption type	380 kg/m³	0.9 MPa

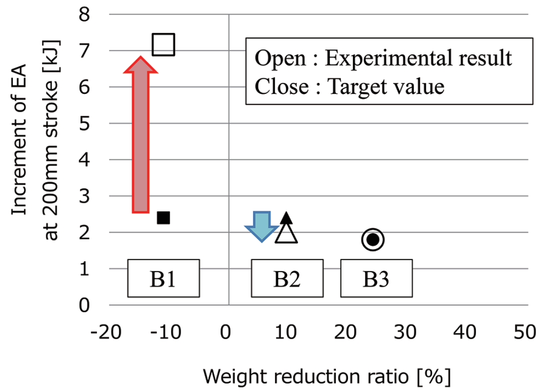

Fig. 8 Absorbed energy increment and weight reduction rate

Table 4 Studied model and weight

Model	B3	B3-5	B3-10	B3-G
Resin material	Urethane foam * 3 times type	Urethane foam * 5 times type	Urethane foam * 10 times type	Urethane foam * Vibrational absorption type
Weight	2.6 kg (−25%)	2.5 kg (−26%)	2.4 kg (−27%)	2.6 kg (−24%)

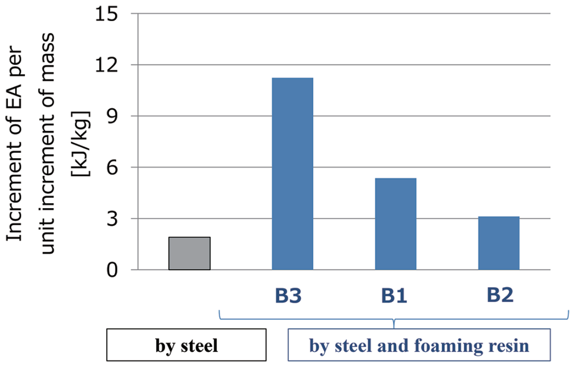

Fig. 9 Absorbed energy increment per unit weight increment

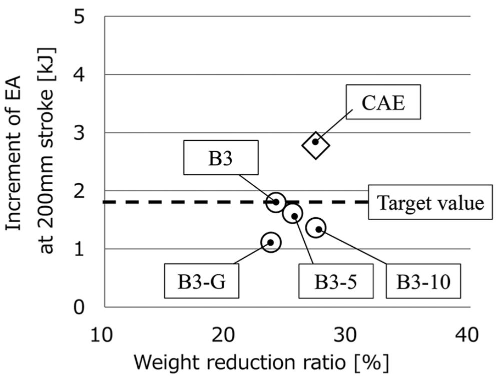

Fig. 10 Absorbed energy increment and weight reduction rate

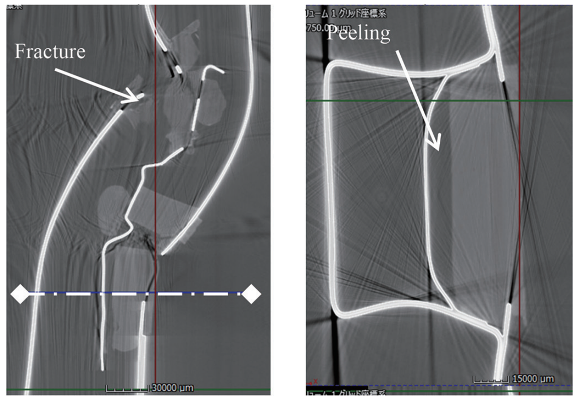

Fig. 11a CT image of model B3 after deformation (50 mm stroke)

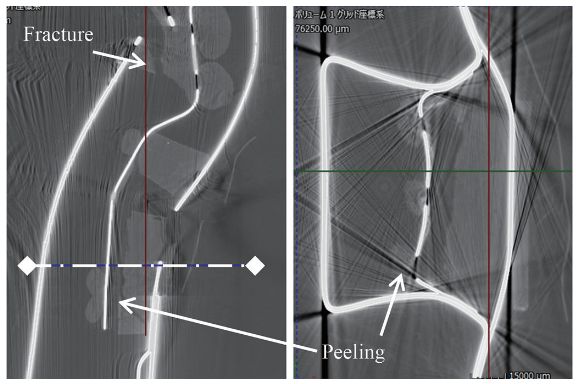

Fig. 11b CT image of model B3-10 after deformation (50 mm stroke)

absorption type) (Table 3). All the foamed resins were made by Sunstar Engineering Inc. For models B3-5, B3-10, and B3-G for which resin materials were applied (**Table 4**), all conditions other than the type of foamed resin were the same as those of model B3. **Figure 10** shows the results along with the results by CAE as reference. The CAE model configuration is the same at that of model B3-10. The deformation behavior of all the models was the same as that of model B3 shown in Fig. 7, but the performance differed. Only model B3 with the 3 times type of resin material achieved the target performance. When the foaming rate was larger, the weight reduction rate was higher, but the performance tended to deteriorate. As a result, the performance of the model with the 10 times type deviated by approximately 1.5 kJ from the CAE model.

The model using the vibrational absorption type was lighter, but it did not meet the target performance. This may be because the compressive elastic modulus of the vibrational absorption type is lower than that of the other resin types. **Figure 11a** is a computed tomography (CT) image of the curvature section of model B3 when the stroke was 50 mm. **Figure 11b** is a CT image of model B3-10. In the images, the white parts are the steel sheets and the gray parts are the resin materials. On both models, when the stroke was 50 mm, the steel sheets separated from the resin and the resin material ruptured. It is indicated that these ruptures are one of the causes of deviation of the experimental values from the simulation results by CAE. Avoiding cracks on the resin material at the early stage and separation of the steel sheet could further reduce the weight of body frames.

3. Development of Lightweight Center Pillars with Higher Crash Performance

3.1 Conditions for side collision

The New Car Assessment Program (NCAP[1, 2]) and various other programs have been used to secure the collision safety of vehicle bodies. The collision safety performance has been evaluated under standard collision test conditions. These programs worked to reduce the number of deaths in car accidents, but in recent years some have considered that this is insufficient and pointed out that severer collision test conditions are necessary. One condition being studied is to increase the impact speed in side collision tests,[4] implemented by the Insurance Institute for Highway Safety (IIHS) in the U.S., by 20% to 60 km/h.[5–7] This paper studied lightweight center pillars under severer impact conditions on the assumption that impact conditions would also have been made severer.

3.2 Calculation of collapse moment

Large loads occur on center pillars (frames) due to side collision. If a center pillar bends at the center area in the longitudinal direction due to such load, damage to passenger(s) is severe, so many vehicles have center pillars that will bend at their lower sections as their structure. However, moment occurring at the center area of a center pillar due to collision develops fast and the moment that causes bending at the center area (hereinafter referred to as the collapse moment) is reached first and thereby the frame easily bends. Therefore, to bend a center pillar at the lower section, the collapse moment at the center area needs to be made higher and the collapse moment at the lower section needs, on the other hand, to be made lower as the structure; or materials need to be arranged appropriately. However, the collapse moment varies depending on the shapes and materials of members, so many researchers studied this aspect in the past.[8, 9]

This paper defines the relationship between the collapse moment (M_c) and fully plastic bending moment (M_p) based on studies by Kimura et al.[10, 11] and studies optimum material arrangement.

$$\frac{M_c}{M_p} = \frac{0.225}{\alpha(1-\alpha)}\left(\frac{t}{b}\right)^2\left(\frac{2kE}{3\sigma_y}\right), \tag{6}$$

$$\frac{M_c}{M_p} = \frac{\alpha(\alpha-1)}{0.9}\left(\frac{b}{t}\right)^2\left(\frac{3\sigma_y}{2kE}\right)+1. \tag{7}$$

Here, t is the thickness of the sheet, b is its width, k is the buckling coefficient, E is Young's modulus, and σ_y is the yield stress. Formula (6) is when $M_c/M_p \leq 0.5$. Formula (7) is when $M_c/M_p \geq 0.5$. When $M_c/M_p = 0.5$, they become continuous. Symbol α is the ratio of yield stress to proportional limit stress. In this paper, it was assumed to be 95% ($\alpha = 0.95$) for all the materials. The buckling constant was determined as 4 in accordance with the document.[9] Although the aforementioned formulas assume a flat sheet, the author assumed that body frames satisfy the same relationship since they are a combination of flat sheets.

3.3 Study of arrangement of materials and thickness considering the collapse moment

Figure 12 shows the distribution of the maximum bending moment (M) to the outer center pillar estimated when the impact speed at the time of side collision is 60 km/h along with the distribution of the collapse moment under the conditions in **Table 5**. **Figure 13** illustrates the shape of an outer center pillar along with the approximate dimensions. The distribution of the maximum bending moment (M) on the outer center pillar was calculated considering the influences of increased speed and weight in reference to the analysis results of side collision of current commercially available C-Segment vehicles. The weight was 1 880 kg (weight of the vehicle: 1 800 kg + human: 80 kg). The estimated value is the maximum at the center area of the outer center pillar, indicating that high moment of approximately 20 kNm may be applied. In addition, the author considered that buckling may first occur on the center pillar outer plane whose distance between the ridgelines was the longest and used the plane as a representative plane to calculate the width (b). Then, the author calculated the distribution of the collapse moment (M_c).

Figure 14 is taken as an example, showing the distribution of the ratio (M_c/M_p) of the collapse moment to the fully plastic bending moment that was calculated from formulas (6) and (7) for model V

Table 5 Placement of tensile strength and thickness in each models

Tensile strength/ Thickness	Model I	Model II	Model III	Model IV	Model V
A	1.5 GPa /1.6 mm	1.5 GPa /2.8 mm	2.0 GPa /2.6 mm	1.5 GPa /3.2 mm	2.0 GPa /2.6 mm
B	1.5 GPa /1.6 mm	1.5 GPa /2.8 mm	2.0 GPa /2.6 mm	1.5 GPa /2.2 mm	2.0 GPa /2.0 mm
C	590 MPa /1.6 mm	590 MPa /2.8 mm	590 MPa /2.6 mm	980 MPa /1.4 mm	980 MPa /1.4 mm

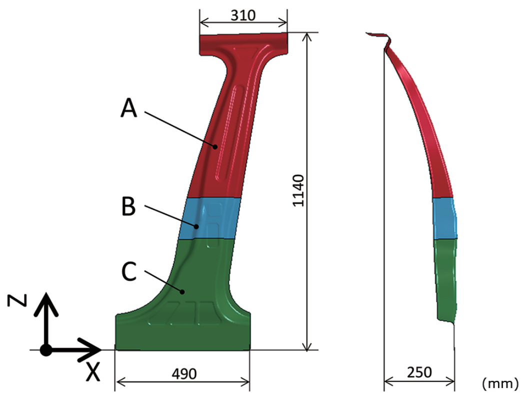

Fig. 13 Center pillar outer model

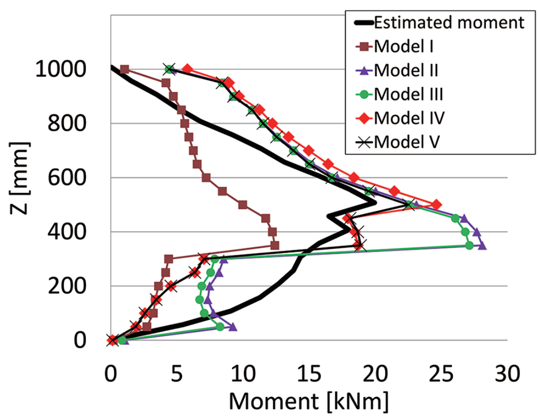

Fig. 12 Estimated maximum bending moment and collapse moment of each models

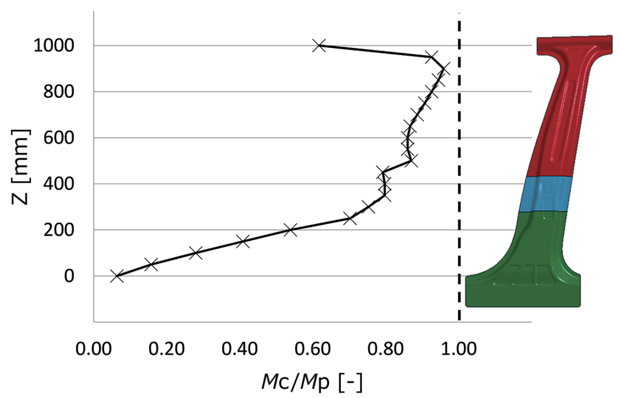

Fig. 14 Distribution of ratio of collapse moment to fully plastic bending moment in model V

in the table. The broken line in the figure is the line on which the collapse moment matches the fully plastic bending moment (M_c/M_p = 1.0). The fully plastic bending moment is the moment around the X-axis (Fig. 13). Figure 14 shows that the ratio is small in the lower area where the width of the representative plane (b) is large, showing that the difference between the fully plastic bending moment and collapse moment is large. In addition, Fig. 13 shows that the collapse moment (M_c) falls below the maximum bending moment (M) in almost all of the areas for model I in the table, indicating that bending is of concern at the center area (area whose height from the lower end (Z) is 400 to 600 mm) where the maximum bending moment is large.

Meanwhile, for models II to V, in the center area and area above it, the collapse moment (M_c) is higher than the maximum bending moment (M), so bending may not occur. For models II to V, the collapse moment (M_c) is lower than the maximum bending moment (M) in the lower area (whose height from the lower end (Z) is up to 300 mm), so bending may occur in their lower areas. For models II and III, the collapse moment is significantly higher than the maximum bending moment in the area whose height from the lower end (Z) is approximately 400 mm, showing that excessive performance is present locally. Therefore, the sheets of models IV and V were partially thinned assuming a tailored welded blank (TWB). As a result, compared with model II whose performance was secured by simply using a thicker sheet, on ultra-high-strength model V whose material and thickness were provided in an optimum way, the weight can be reduced by as much as 29% (**Fig. 15**).

3.4 Verification of lightweight center pillars by CAE

The appropriateness of the lightweight outer center pillar (model V in Table 5) described in the previous section was verified by CAE. The boundary condition was simulated on side collision (**Fig. 16**). The impact speed (initial velocity) of an impactor assumed as the rigid body in the figure was 20 km/h and the weight was approximately 1 700 kg. Under these conditions, the moment to be applied to the center pillar was examined. As the test piece, an inner center pillar was combined with the outer center pillar. The assumed inner center pillar was a 1.0-mm-thick steel sheet with a tensile strength of 980 MPa. The load moment that the inner center pillar bears was added as a target and it was determined that, even when a load moment around the X-axis of up to 24 kNm is applied to the center pillar, the center area does not bend.

Figure 17 shows the distribution of the load moment simulated by CAE. The broken line in the figure shows the target moment (24 kNm). The figure shows that, as time passes, the moment occurring at the center area increases to the maximum. It becomes the maximum in approximately 36 ms after collision. The maximum moment finally exceeds 24 kNm, showing that the load moment assumed to occur in a side collision test of a vehicle body at a speed of 60 km/h can be given from the aforementioned boundary condition and model V. **Figure 18** shows the deformation behavior. The figure shows that deformation is concentrated in the lower section and bending occurs. It also shows that no bending occurs at the center area. Therefore, it shows that the lightweight center pillars studied in the previous section are expected to have high crash performance under severer collision conditions.

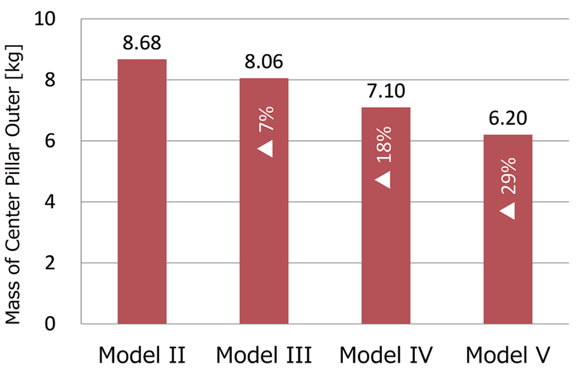

Fig. 15 Weight and lightening rate of each models

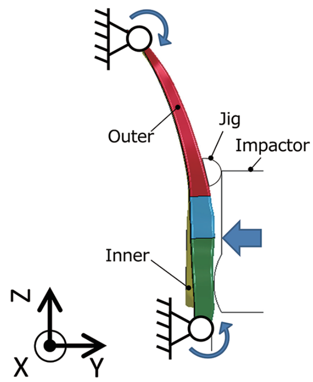

Fig. 16 Condition of side impact crash simulation

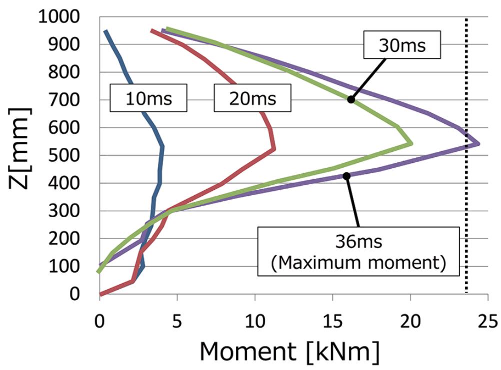

Fig. 17 Moment distribution of center pillar

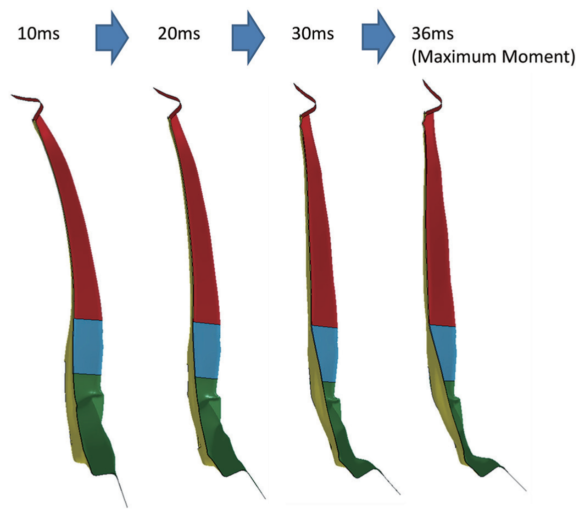

Fig. 18 Deformation behavior of center pillar

4. Conclusions

This paper studied weight reduction of front side members and center pillars. The author has proposed front side members for which foamed resin materials are used combination to suppress out-of-plane deformation, which may deteriorate the performance due to thickness reduction, achieving approximately 25% weight reduction without changing the deformation behavior. Regarding the center pillars, the author has proposed the optimum arrangement of materials, realizing lightweight center pillars that satisfy severe collision conditions.

To further reduce the weight, combination with fundamental technologies described in this paper may be more important in place of simple replacement of materials. Nippon Steel will pursue necessary fundamental technologies to contribute to increasing needs for collision safety and lower environmental stress.

Acknowledgments

I express my sincere gratitude to Mr. Toshio Kobayashi and Mr. Hiroyuki Nagata, Chemical Research and Development Department of Sunstar Engineering Inc., who assisted in filling with resin materials when lightweight FSMs were prepared.

References

1) Frontal Full-Wrap Collision Safety Performance Test Procedures. 2018, http://www.nasva.go.jp/mamoru/download/H30-01.pdf
2) Frontal Offset Collision Safety Performance Test Procedures. 2018, http://www.nasva.go.jp/mamoru/download/H30-02.pdf
3) von Karman, T. et al.: Trans. ASME. 54, 53 (1932)
4) IIHS Side Impact Crash Test Protocol. Version X, 2017, https://www.iihs.org/media/ebc9bd1f-2ca4-4fb9-b96e-f4165f331943/Jil- Xg/Ratings/Protocols/current/test_protocol_side.pdf
5) Brumbelow, M.L. et al.: Proceedings of the 25th International Technical Conference on the Enhanced Safety of Vehicles (ESV). 2017
6) Reichert, R. et al.: Proceedings of the 15th International LS-DYNA Users Conference. 2018
7) Mueller, B.C. et al.: Proceedings of the 14th International Symposium on Sophisticated Car Occupant Safety Systems. 2018
8) Koga, A. et al.: Transactions of Society of Automotive Engineers of Japan. 49 (6), 1255 (2018)
9) Niwa, K. et al.: 2015 JSAE Annual Congress (Autumn) Proceedings. No.51-15A, 1222 (2015)
10) Kimura, M. et al.: Journal of Structural and Construction Engineering (Transactions of AIJ). 545, 135 (2001)
11) Inoue, T. et al.: Journal of Structural and Construction Engineering (Transactions of AIJ). 527, 205 (2000)

Satoshi HIROSE
Senior Researcher, Ph.D.
Kimitsu R & D Lab.
1 Kimitsu, Kimitsu City, Chiba Pref. 299-1141